Investigation of the Kinetics of Fluidized Bed Spray Agglomeration Based on Stochastic Methods

Korina Terrazas-Velarde, Mirko Peglow, and Evangelos Tsotsas
Dept. of Thermal Process Engineering, Otto von Guericke University, Magdeburg 39106, Germany

DOI 10.1002/aic.12506
Published online February 1, 2011 in Wiley Online Library (wileyonlinelibrary.com).

Particle formation during fluidized bed spray agglomeration is modeled by a Monte Carlo method. The methodology is based on the micromechanisms occurring within the bed. The most important model parameters are identified as interparticle collision time, deposited droplet drying time and droplet addition time. It is found that a high number of collisions leads to a negligible role of the drying mechanism. In the real bed, however, the process is dependent on the gas inlet temperature. This indicates that the number of collisions relevant to agglomeration is relatively low. The accordance of the model with experimental results for variations of several process parameters demonstrates that the approach is a promising way to simulate the formation of agglomerates. In addition, the model is able to reproduce slower agglomeration at increased temperatures. This result is, for the first time, based on physical mechanisms rather than on the use of fitted agglomeration kernels. © 2011 American Institute of Chemical Engineers *AIChE J,* 57: 3012–3026, 2011
Keywords: drying, fluidization, agglomeration, stochastic modeling, Monte Carlo method

Introduction

Agglomeration is a technology by which particles are joined together in a random way leading to porous aggregates much larger than the original material and with different properties. Many consumables such as fertilizers, medicaments or food products are manufactured by agglomeration.[1] Fluidized spray agglomeration is one of the most used techniques due to its versatility and the easy combination of liquid distribution and drying in a single apparatus.[2] The process consists in the atomization of a liquid feed onto a fluidized bed of solid particles. The bed movement causes the formation of liquid bridges between the individual particles. These bridges are dried by the fluidization gas resulting in solid junctions that allow the particles to grow.

The final agglomerate properties depend on the operating conditions during agglomeration, for example on the nature and amount of binder used, the way it is introduced to the system or the drying conditions. On the other hand, these properties must fulfill end-user requirements. The food industry, e.g., aims at good agglomerate solubility and dispersibility in liquids, which are normally achieved by high agglomerate porosities and low densities.[3] The agglomerates should, however, be strong enough to withstand handling and transportation. Pharmaceutical agglomerates should exhibit good wettability. Additionally they should have an internal structure that allows for direct compression in tabletting machines.[4] Better understanding of the agglomeration process is necessary for producing the desired end-user properties at low cost and improving equipment design. Despite extensive study of heat and mass transfer between the

Correspondence concerning this article should be addressed to K. Terrazas-Velarde at korinaterrazas@yahoo.com.mx.

involved phases and the development of efficient methods for the description of size enlargement by population balances,[5–7] there is still a lack of knowledge on how the different mechanisms occurring during the formation of agglomerates are interrelated. Such interactions become accessible by use of microlevel approaches,[8] but they are not yet fully described. Therefore, the stochastic microlevel approach is further developed in this article, focusing on competing phenomena and thermal effects.

The present solution method is based on the use of random numbers and probabilities to simulate the agglomeration process of a finite number of primary particles. It is a Monte Carlo (MC) method[9] that represents the stochastic numerical solution of the population balances equations.[10] An important advantage of MC is that less mathematical effort is required in comparison to the traditional deterministic methods. Since the MC method is by nature discrete, no discretization is necessary. Moreover, the uncertainties of choosing among various agglomeration kernels is avoided. Limitations exist in the number of particles that can be simulated. It has been found that up to 10^4 particles can be modeled with the nowadays available desktop computer power and that even a relatively small number of 10^3 particles is enough to achieve very good accuracy at a reasonable computational speed.[11] In this study, an event driven method with periodical particle regulation called Constant Volume MC method is used. The method was found to be the most suitable for coalescence dominated processes. Under this methodology an event occurs first and then time is advanced in an appropriate amount. The number of entities (primary particles or agglomerates) decreases as the simulation proceeds. Once the number of particles in the simulation box reaches half of the initial number, an exact copy of the particle population is introduced to the simulation box restoring the number of entities to the initial value.

The approach is based on the study of the individual interactions taking place between particles and droplets, and treats the formation of agglomerates as a network of micromechanisms that occur in series and parallel.[12] The initiating mechanism in terms of agglomeration is droplet deposition or wetting of the particle surface. Then, the fluidized bed movement forces the particles to collide. The first possible scenario is that the particles touch each other on at least one wet region. Under these conditions a coalescence may be observed if the liquid layer is able to completely absorb the collision kinetic energy by viscous dissipation. This leads to the formation of a liquid bridge that eventually solidifies by solvent evaporation in the fluidization gas. Breakage of the already formed agglomerates may be observed when the liquid or solid bridges break apart due to collision forces. The second scenario occurs when the deposited droplet does not contact the surface of another particle or when particle rebound is observed. In these cases, the droplet may have enough time to dry and vanish, reducing in this way the agglomeration efficiency of the process.

The probability of each of the two scenarios to occur is not only a function of the layer ability to dissipate the collision energy but also of the elapsed time between collisions (collision time) and the characteristic drying time of the deposited droplet. As it can be easily inferred, the more collisions that a particle undergoes per unit time, the higher is the probability of a successful coalescence assuming that all other parameters are kept constant. This means that, with an infinite number of particle collisions, the mechanism of drying of the deposited droplets will be impeded because all accessible droplets will be consumed to form a liquid bridge before they dry out. Under these conditions, the highest achievable agglomeration rate will be observed. On the other hand, with a very small number of collisions the droplets would already be dried before a subsequent collision takes place, hindering any agglomeration. An additional important parameter that also rules the speed of the agglomeration process is the characteristic droplet addition time. When this quantity is small, faster agglomeration is expected. Then, the net agglomeration rate will be the result of the relationship between these three characteristic quantities, namely collision time, drying time and addition time. The microlevel approach allows, contrary to the PBE solutions, to analyze this relationship and its influence on the size enlargement process. This work attempts to provide a basis for this analysis and to demonstrate the implications of drying during the formation of agglomerates based on physical principles.

Computational Method

General algorithm

The simulation corresponds to a batch process in which the fluidization gas mass flow rate is held constant. The fixed bed voidage ε_{fix} is assumed equal to 0.4 corresponding to a random packing of uniform-sized spheres.[13] Once fluidization is started, the bed reaches its maximum voidage ε_{exp} which depends on the gas velocity u_0 and particle properties[14] as

$$\varepsilon_{exp} = \left(\frac{18\ \mathrm{Re_p} + 0.36\ \mathrm{Re_p}^2}{\mathrm{Ar}} \right)^{0.21} \tag{1}$$

Here, $\mathrm{Re_p}$ and Ar are the particle Reynolds and Archimedes dimensionless numbers defined by

$$\mathrm{Re_p} = \frac{u_o \rho_g d_p}{\mu_g}, \tag{2}$$

$$\mathrm{Ar} = \frac{{d_p}^3 \rho_g (\rho_p - \rho_g) g}{{\mu_g}^2}. \tag{3}$$

As agglomeration proceeds and particles become larger, the expanded bed voidage decreases. This is accompanied by the contraction of the bed from its maximum height to the fixed bed height. Once the voidage of the expanded bed is equal to that of the fixed bed, the simulation is stopped and the bed is assumed to collapse.

The simulation box should be understood as a representative sample of the particle population with a finite number of particles. An event k is treated as a pair-wise collision i between particles. For that, the entire population is randomly divided into two main groups with $i = N_p/2$ number of pairs. Then, the first and second coalescence conditions (collision on a wet spot and fulfillment of the Stokes criterion, respectively) as well as the breakage criterion are verified for each ith pair of particles. By following this procedure, it is

decided whether the individual pair collision will lead to an agglomeration, breakage or rebound event (the latter simply represented by a nonagglomeration and nonbreakage event). At the end of all pair collisions i, the population undergoes a granulometric analysis to determine its median diameter d_{50}. Based on the new diameter, the bed properties are recalculated and the next event (k+1) is computed. With this methodology, the main parameter in the simulation is not time but the number of events k happening in the agglomerator. Once the simulation is finished, the transient behavior of the agglomerate diameter and the decrease of total number of entities in the simulation box are obtained. This procedure provides at all times the number of particles forming each agglomerate; therefore, the particle size distribution can be easily obtained.

Droplet addition

The relationship between real process and model is established by the concentration of droplets per unit time and particle inside the simulation box. The number of droplets added per unit time in the real process, which depends on the liquid flow rate and the droplet diameter, is

$$\dot{N}_{\mathrm{d}} = \frac{6\,\dot{M}_{\mathrm{l}}}{\pi\,\rho_{\mathrm{l}} {d_{\mathrm{d}}}^3}. \tag{4}$$

Consequently, the number of droplets per particle and unit time is

$$\gamma = \frac{\dot{M}_{\mathrm{l}}}{M_{\mathrm{bed}}} \left(\frac{\rho_{\mathrm{p}}}{\rho_{\mathrm{l}}}\right) \left(\frac{d_{\mathrm{p}}}{d_{\mathrm{d}}}\right)^3. \tag{5}$$

By means of the droplet addition rate γ and the number of particles within the simulation box N_{p}, the droplet addition time t_{ad}, which physically designates the time necessary to add a single droplet to the simulation box, is calculated to be

$$t_{\mathrm{ad}} = \frac{1}{2^{\mathcal{N}} \gamma\, N_{\mathrm{p},0}}, \tag{6}$$

where $\mathcal{N}$ is the number of doublings that the simulation system undergoes according to the CVMC method.

Once a droplet is introduced to the simulation box, the particle to be wetted is chosen randomly among the entire population. Droplets and primary particles are assumed monosized, the droplet diameter d_{d} being smaller than the particle diameter d_{p}. This allows the wetting mechanism to be modeled in terms of increasing fractional coverage of the particle surface that can be calculated by

$$\Phi_{\mathrm{s}} = \frac{a^2}{{d_{\mathrm{p}}}^2}. \tag{7}$$

Here, a is the base radius (foot print) of the spherical cap of given volume $V_{\mathrm{d}} = V_{\mathrm{cap}}$ and contact angle θ, which can be obtained by the relationship[15]

$$a = \left(\frac{3\,V_{\mathrm{cap}}}{\pi} \frac{\sin^3\,\theta}{2 - 3\,\cos\,\theta + \cos^3\,\theta}\right)^{1/3}. \tag{8}$$

Then, the number of positions p available for droplets on the primary particle surface is calculated as

$$p = \frac{1}{\Phi_{\mathrm{s}}}. \tag{9}$$

The droplet is deposited on an empty position chosen randomly among the positions of the primary particles forming the agglomerate (no overlapping of droplets is considered). As the particles coalesce, the number of positions per agglomerate increases according to the number of constituent primary particles. This means, the bigger the agglomerate, the higher is its droplet capture probability. The effect of sterically impeded droplets, or droplets that can not be accessed after a successful coalescence due to the agglomerate spatial structure, is included based on the assumption of a maximum coordination number equal to 6.

Coalescence criterion

Colliding agglomerates coalesce if their initial kinetic energy is too small to overcome the viscous lubrication resistance in the liquid layer. Ennis et al.[16] first derived the critical conditions for the dissipation of kinetic energy by a viscous layer of a given thickness as

$$St_{\mathrm{coal}} = \frac{2\,M_{\mathrm{agg}} u_{\mathrm{c}}}{3\,\pi \mu_{\mathrm{l}} {d_{\mathrm{agg}}}^2}, \tag{10}$$

where the combined particle mass and diameter are described by

$$M_{\mathrm{agg}} = \frac{2 M_{\mathrm{agg1}} M_{\mathrm{agg2}}}{M_{\mathrm{agg1}} + M_{\mathrm{agg2}}}, \tag{11}$$

$$d_{\mathrm{p}} = \frac{2 d_{\mathrm{agg1}} d_{\mathrm{agg2}}}{d_{\mathrm{agg1}} + d_{\mathrm{agg2}}}. \tag{12}$$

A collision is assumed to be successful if the particles touch each other at a wet position (1st agglomeration condition) and if the Stokes number is below a certain critical value (2nd agglomeration condition) given by

$$St^*_{\mathrm{coal}} = \left(1 + \frac{1}{e}\right) \ln\left(\frac{h}{h_{\mathrm{a}}}\right), \tag{13}$$

where e is the particle restitution coefficient and h is the maximum height of the binder layer calculated by

$$h = a \frac{1 - \cos\theta}{\sin\,\theta}. \tag{14}$$

The Stokes model strongly depends on the particle collision velocity. As the superficial gas velocity u_0 has been found to be directly related to the bed turbulence and thus to the particle collision velocity u_{c},[17] in this study, the collision velocity of the pair of particles is randomly chosen assuming a normally distributed function around a mean value equal to 0.5 u_0 with a standard deviation of 0.1 m/s.

Deposited droplet drying

For the description of this phenomenon, the particles are considered to be nonporous. Additionally, binder layer height

and radius are assumed to diminish simultaneously, maintaining the contact angle constant.[18] Under these conditions, the transient change of the molar amount of water N_w contained in the deposited droplet with time is described by

$$\frac{dN_w}{dt} = 3\frac{\rho_w}{\tilde{M}_w}\pi\left[\frac{1}{1-\cos\theta}-\frac{1}{3}\right]h^2\frac{dh}{dt}. \quad (15)$$

The same quantity can be obtained on kinetic terms to

$$\frac{dN_w}{dt} = A_{cap}\beta\frac{\rho_g}{\tilde{M}_g}(\tilde{y}^* - \tilde{y}_g), \quad (16)$$

where β is the mass transfer coefficient, $\tilde{y}^*$ is the vapor molar fraction at saturation conditions $\tilde{y}^* = P_v^*/P$ and $\tilde{y}_g$ is the vapor molar fraction in the bulk of the gas.

Combining Eq. 15 with 16 and assuming constant β , the expression for the reduction of the binder layer height h is obtained as follows

$$h = h_o - \frac{2}{3}\frac{\rho_g}{\rho_w}\frac{\tilde{M}_w}{\tilde{M}_g}\frac{\beta}{1-\cos\theta}\left(\frac{P_v^*}{P}-\tilde{y}_g\right)\left[\frac{1}{1-\cos\theta}-\frac{1}{3}\right]^{-t}t. \quad (17)$$

Here, P is the system pressure and P_v^* is the saturation pressure of water calculated by the Antoine equation at adiabatic saturation temperature T^*.

Assuming that the fluidized bed is a well mixed medium and that the amount of evaporating water is at any time equal to the amount of sprayed water, the moisture content in the gas Y_g can be calculated as

$$Y_g = Y_{g,in} + \frac{\dot{M}_w}{\dot{M}_g}, \quad (18)$$

where $\dot{M}_g$ and $\dot{M}_w$ are the mass flow rates of gas and water, respectively.

Vapor molar fraction is related to the vapor moisture content in the gas according to the equation

$$\tilde{y}_g = \frac{Y_g}{Y_g + \frac{\tilde{M}_w}{\tilde{M}_g}}. \quad (19)$$

Equation 17 describes the reduction by drying of the initial binder layer height h_0 of a droplet deposited on a solid nonporous particle as a function of time, temperature, fluidization velocity (implicit in the mass transfer coefficient), contact angle, particle, binder and fluidization gas properties.

The mass transfer coefficient β is calculated for the initial conditions from standard correlations for the Sherwood number.[19] Therein, the characteristic length l is the ratio between mass transfer area and the projection perimeter in gas flow direction, considering the deposited droplet as a semiellipse. For a side-flow we obtain

$$l = \frac{2\,{h_0}^2}{1-\cos\theta}\left(\frac{2}{{a_0}^2+{h_0}^2}\right)^{1/2}, \quad (20)$$

and for a top-flow

$$l = \frac{{h_0}^2}{a_0(1-\cos\theta)}. \quad (21)$$

However, for a droplet deposited on a fluidized particle, the flow direction is not limited to one of these conditions. Therefore, the characteristic length was set to

$$l = d_{d,0}. \quad (22)$$

Initially, the deposited droplet has a binder mass fraction

$$x_{b,0} = \frac{M_b}{M_b + M_{w,0}}, \quad (23)$$

where M_b and $M_{w,0}$ are the mass of solute and the initial amount of liquid (water) in the solution, respectively. The mass of solute in the binder solution is fixed for each initial mass fraction and cap volume as

$$M_b = x_{b,0}\,V_{cap,0}\,\rho_l, \quad (24)$$

where ρ_l is the density of the binder solution, which is slightly higher than the water density ρ_w. As the droplet dries, the mass of solute M_b remains constant and the amount of water M_w decreases, this results in an increase of solute mass fraction x_b and, therefore, in an increase of solution viscosity μ_l.

The mass of liquid remaining in the droplet M_w is calculated at each time step based on the remaining cap volume V_{cap} as

$$M_w|_t = \rho_w\,V_{cap}|_t = \rho_w\,\pi\left[\frac{1}{1-\cos\theta}-\frac{1}{3}\right]h^3|_t. \quad (25)$$

Thereafter, the instantaneous average binder mass fraction is given by

$$x_b|_t = \frac{M_b}{M_b + M_w|_t}. \quad (26)$$

To introduce the change of viscosity due to drying to the model, a relationship between binder mass fraction and binder viscosity is necessary.

Interparticle collision frequency

The collision frequency allows to calculate the length of the time step during the simulation and, thus, to correlate the real with the computational time. In this study, the empirical correlation proposed by Buffière and Moletta[20] is used to estimate the frequency of collisions within the fluidized bed

$$f_{coll} = F_{coll}\left[1-\left(\frac{\phi_{exp}}{\phi_{fix}}\right)\right]\left(\frac{\phi_{exp}}{\phi_{fix}}\right)^2 u_0 \quad (27)$$

where F_{coll} is the collision frequency prefactor. This is prefactor that was adjusted to quantitatively follow the experimental observations, showing a value of 56400 in the work of Buffière and Moletta. The correlation (u_0 in m/s and f_{coll} in 1/s) describes the behavior of the number of collisions that a particle experiences per unit time as the fluidized bed

moves from the elutriation limit ($\phi_{exp} \approx 0$; $\varepsilon_{exp} \approx 1$) to the packed bed limit ($\phi_{exp} \approx 0.6$; $\varepsilon_{exp} \approx 0.4$) with particle growth.

To advance the simulation in real time, a number of events k is set at the beginning of the simulation. As the events occur one after the other, the collision frequency is calculated and the length of the time step for each collision is set to

$$t_{step} = \frac{1}{f_{coll}}. \tag{28}$$

Recall that each event k contains i pair-wise collisions that are assumed to occur simultaneously. Once the simulation is finished (desired number of events k is reached), the real time t_{real} elapsed for the simulated collisions can be set to

$$t_{real} = \sum_{k=1}^{k} t_{step} \tag{29}$$

The length of the time step is not constant during the simulation, due to the change of the expanded solid volume fraction ϕ_{exp} as agglomeration proceeds at constant superficial velocity u_0.

Experimental Method

Deposited droplet drying experiments

Gas velocity Effect. The effect of gas velocity on drying was checked in Terrazas-Velarde et al.[8] There, single droplet drying experiments at constant ambient temperature $T_g = 20°C$ and various gas velocities ($u_0 = 0.8$, 1.2, and 1.4 m/s) are presented. The pure water droplets had a mean volume of $V_d = 0.75$ μl and were deposited on a glass surface by a calibrated micropipette. The gas was air with a moisture content less than 0.4 g/kg. The air flow was adjusted by a valve and delivered by a flexible tube. The end of the tube was placed ~1 cm from the droplet in side-flow configuration. Air velocity and temperature were measured by a thermal anemometer. The drying process was recorded by a medium-speed camera. The reduction of the maximum height of the spherical cap as a function of time was monitored by image analysis.

However, the conditions of the single droplet experiment may significantly differ from the drying conditions present in the fluidized bed, and this is not accounted for in Terrazas-Velarde et al.;[8] In the single droplet drying experiments, the air is almost dry and no continuous addition of liquid to the system is observed. Therefore, the molar fraction of vapor in the gas phase $\tilde{y_g}$ can be assumed to be zero. For the calculation of the mass transfer coefficient, the characteristic length of Eq. 20 is used, as it corresponds with the experimental side-flow configuration. In the fluidized bed, however, the flow pattern is not restricted to this condition, so that the use of Eq. 22 may be more accurate. A major difference exists in the calculation of the saturation vapor pressure P_v^*, which is a function of droplet temperature. For the drying conditions of the single droplet experiments this temperature is likely to be much closer to the gas temperature T_g than to the adiabatic saturation temperature T^*. Figure 1 presents the comparison of the experimental results with the drying model given by Eq. 17 at "single droplet" (SD) conditions, ($\tilde{y_g} = 0$ and P_v^* calculated at $T_g = 20°C$) and at "fluidized bed" (FB) conditions ($\tilde{y_g}$ calculated by Eq. 19 and P_v^* calculated with T^*).

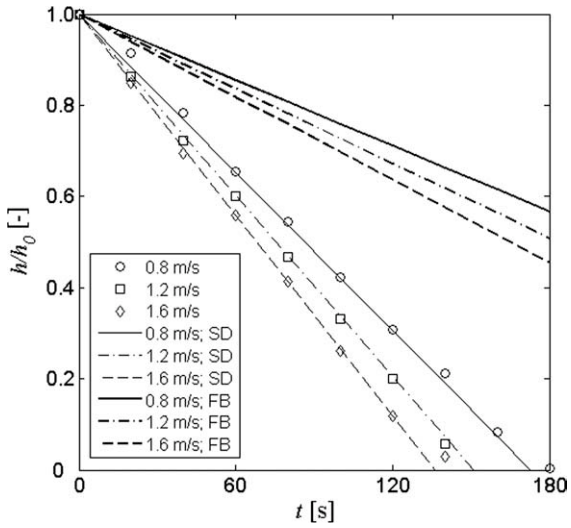

Figure 1. Measured and calculated droplet heights; Effect of superficial gas velocity.

As it can be seen, the model agrees very well with the experimental results at SD conditions. This suggests that, indeed, the temperature of the droplet is very close to the gas temperature and to the substrate temperature (glass surface) for a single deposited droplet. This is not expected to occur in the fluidized bed, as under real agglomeration process conditions the whole mass of water injected to the system in form of droplets is simultaneously evaporated. Under these conditions, the adiabatic saturation temperature is very likely to be reached. This analysis demonstrates that the drying model proposed in this study is able to follow the experimental tendencies of single droplet experiments. The drying of deposited droplets in the fluidized bed is modeled with the relevant drying conditions as already described.

Temperature Effect. The effect of gas temperature was studied by depositing droplets of water on a glass surface and drying them with constant gas velocity $u_0 = 4.1$ m/s at two different temperatures, $T_g = 23°C$ and $T_g = 70°C$. The micropipette was calibrated to produce droplets of $V_d = 1$ μl. The air current was positioned in top-flow configuration. Side-flow was not achievable due to the large distortions of the equilibrium shape at the used large air flow. The air was heated to the desired temperature by an electrical heater. The outlet of the heater was positioned directly over the deposited droplet at a distance of ~5 cm. Figure 2 shows the comparison of the experiments with the drying model at "single droplet" conditions. In the calculations, Eq. 21 is used to obtain the characteristic length l (top flow configuration). As it can be seen, the model correctly describes the decrease of the drying time as the gas temperature increases. The agreement is better at $T_g = 23°C$ whereas that at $T_g = 70°C$ an overestimation of the drying rate of the droplet is observed. This is attributed to the influence of the glass surface (which is initially at ambient temperature) on the drying process. This influence is stronger at higher temperatures

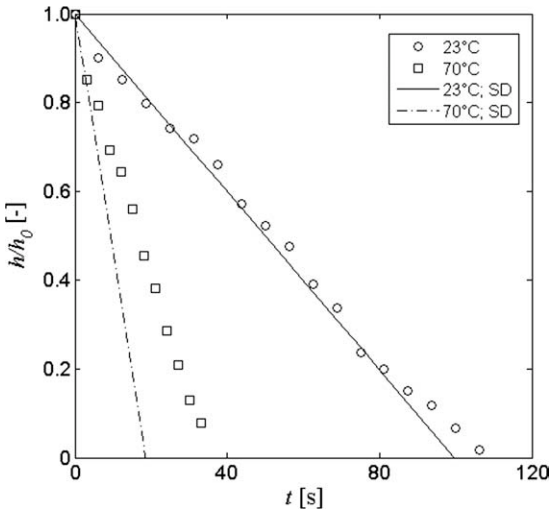

Figure 2. Measured and calculated droplet heights; Effect of gas temperature.

and causes the droplet to dry slower. However, in the fluidized bed, the particles (substrate) have a temperature equal to the temperature of the fluidization gas; therefore, the model is expected to be more accurate.

Lab-scale agglomeration experiments

Binder Properties. Hydroxypropyl-methylcellulose, HPMC (trade name Pharmacoat® 606, from Shin-Etsu, Japan) in aqueous solution was used as binder. The viscosity of HPMC solutions depends strongly on solute concentration as it is shown in Figure 3. On contrary, other properties such as density and surface tension do not vary significantly with the mass fraction of solute.[21,22] Regarding the rheological behavior of the solution, only slight deviations from Newtonian behavior are observed for mass fractions above 12%. From this point on, the solutions exhibit pseudoplastic behavior[22] where the apparent viscosity slightly decreases as

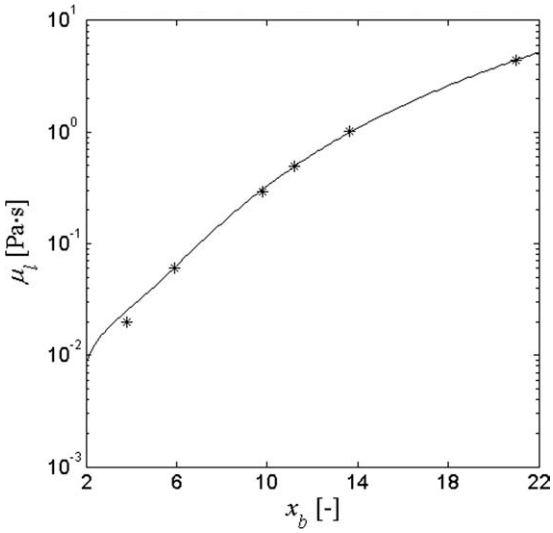

Figure 3. Binder viscosity as function of solute mass fraction.

Table 1. Properties of the Glass Beads

Parameter	Value	Units
d_{50}	0.40	mm
ψ	0.97	–
E	0.80	–
ρ_p	2400	kg/m^3
h_a	10	mm

the rate of shear increases. Since the limiting concentration for successful atomization of the solution lies at mass fractions close to 12%,[23] it is not expected that deviations from Newtonian behavior would affect the process.

Solid Properties. The experiments were performed with glass beads supplied by Cerablast, Germany; their properties are listed in Table 1. The number density q_0 and the cumulative size distribution Q_0 was obtained by a Camsizer 0135, Retsch Technologies, Germany. Figure 4a shows the particle size distribution and the appearance of the beads. The median particle diameter $d_{p,0} = d_{50}$ was obtained from Q_0. The particle sphericity ψ was also obtained by the Camsizer.

Regarding the restitution coefficient, it is reported in literature lo lie between 0.9 and 0.7 depending on glass

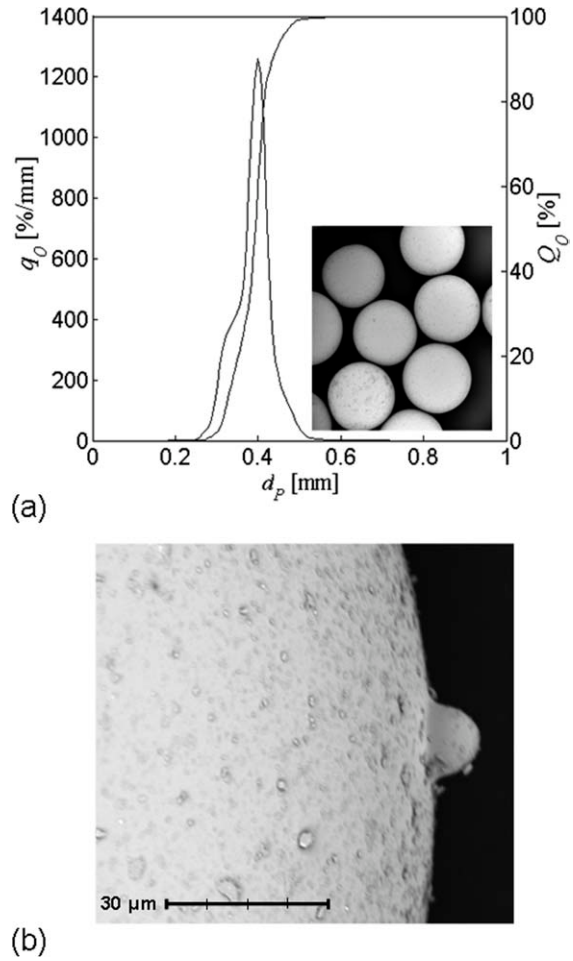

Figure 4. Initial particle size distribution and appearance of glass particles (a); Distinct asperities on the surface of glass particles (b).

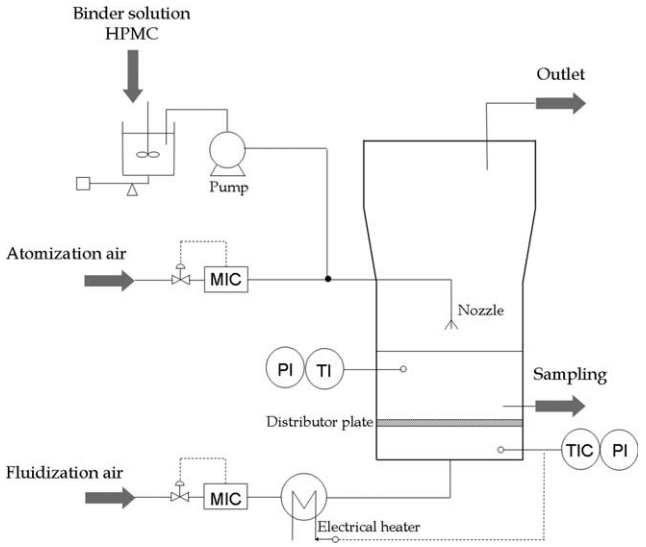

Figure 5. Lab-scale fluidized bed agglomerator.

composition, impact velocity and angle of impact.[24,25] For the sake of simplicity, a value of 0.8 was taken. The density of the solid was calculated from bed density to a value that agrees well with literature.[26,27] The otherwise smooth surface of the glass particles had easily distinguishable asperities of $\sim$10 μm in height, see Figure 4b.

Experimental Setup. Agglomeration experiments were carried out in a lab-scale fluidized bed plant schematically shown in Figure 5. The cylindrical agglomeration chamber has a diameter of 15 cm and a height of 45 cm and is made of Plexiglas. The spray nozzle is a two-fluid nozzle provided by Schlick, Germany, Model 970/0-S4. It was positioned 15 cm above the distributor plate (top spray configuration). The throughput of the binder solution was controlled by a piston pump. Additionally, a balance was used for the online measurement of the sprayed amount.

During agglomeration, samples were taken every 30 s approximately 3 cm above the distributor plate by means of a transversally placed tube. The agglomerate mean diameter and particle size distribution were measured offline by the Camsizer 0135, Retsch Technologies, Germany. Pressurized air was used as the fluidization and atomization gas. The desired fluidization gas inlet temperature was reached by means of an electrical heater. The mass flow rate of the gases was adjusted by mass flow controllers (Bronkhorst, Germany). The experiments were carried out with a batch of 500 g of particles. Variations of binder addition rate, fluidization velocity and gas inlet temperature were performed. The main experimental parameters are shown in Table 1. The experiments were performed until the bed defluidized.

Table 2. Experimental Parameters

Variable	$\dot{M}_g$ (kg/h)	$\dot{M}_l$ (g/h)	$T_{g,in}$ (°C)	u_0 (m/s)	x_b (−)	Label
$\dot{M}_l$	100	**100**	30	1.35	8	E.01
	100	**300**	30	1.35	8	E.02
	100	**500**	30	1.35	8	E.03
x_b	100	300	30	1.35	**4**	E.04
	100	300	30	1.35	**8**	E.02
	100	300	30	1.35	**10**	E.05
u_0	**70**	300	30	**0.94**	8	E.06
	100	300	30	**1.35**	8	E.02
	110	300	30	**1.47**	8	E.07
$T_{g,in}$	100	300	**30**	1.35	10	E.05
	95	300	**50**	1.35	10	E.08
	87	300	**80**	1.35	10	E.09

Table 3. Simulation Parameters for the Investigation of the Effect of F_{coll}

Label	F_{coll} (m^{-1})	$f_{coll,0}$ (s^{-1})	$t_{step,0}$ (s)
S.M01	56400	8812	0.000113
S.M02	5640	881	0.00113
S.M03	2820	440	0.00227
S.M04	640	100	0.010
S.M05	320	50	0.020
S.M06	180	28	0.036
S.M07	40	6.2	0.160
S.M08	10	1.58	0.632
S.M09	2.50	0.40	2.560
S.M10	0.75	0.12	8.534

Results and Discussion

Model sensitivity to characteristic collision, drying and addition times

Collision frequency is given in the present work by the empirical correlation of Eq. 27. This relationship describes the number of collisions that a single particle experiences per unit time and gives the length of the time step (Eq. 28). As it can be inferred, the number of collisions strongly affects the agglomeration rate of the process.

To investigate the extent of the influence of length of the time step (collision time) on the model results, a "base case" was selected from the experiments which corresponds to experiment E.02 in Table 2 (moderate binder spray rate at low temperature). Then, all parameters were set to the corresponding values of E.02 and variations of the collision frequency prefactor were carried out. The tested prefactors are given in Table 3 going from the value of $F_{coll} = 56400$ (in the original work of Buffière and Moletta[20]) to very small values close to zero. This last table also presents the collision frequency f_{coll} (number of collisions per particle per second) for the given F_{coll}, as well as the initial length of the time step t_{step} (time necessary for one single collision). Additional simulation parameters follow the values given in Table 4 corresponding to experiment E.02. The contact angle

Table 4. Additional Simulation Parameters for the Base Case

Parameter	Value	Units
d_d	80	mm
γ	0.05	1/s
θ	40	°
μ_l	0.147	Pa s
u_c	0.675	m/s
T^*	14	°C
$\bar{y_g}$	0.0054	–
Y_g	3.4	g/kg
$N_{p,0}$	2000	–

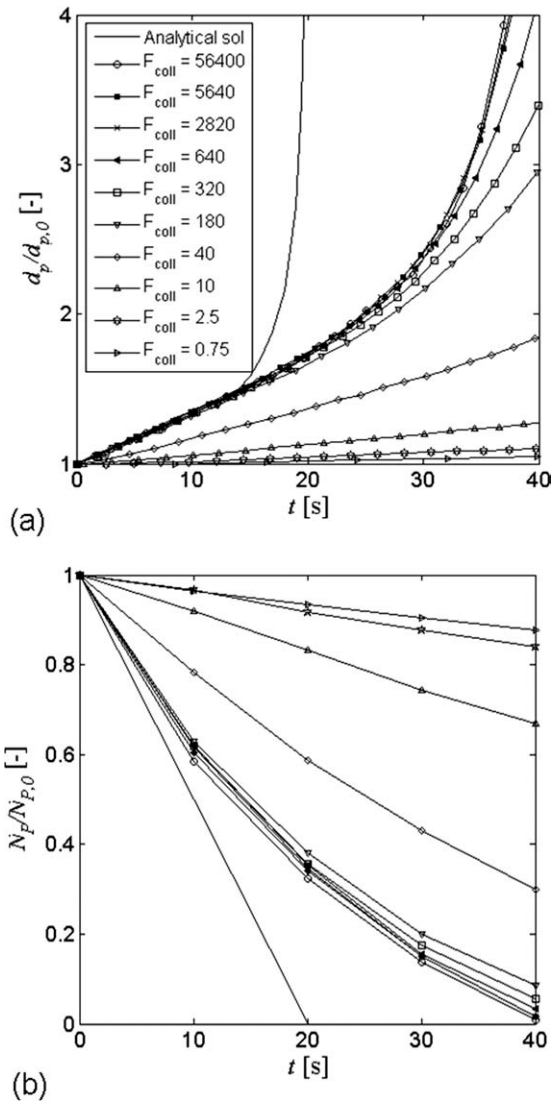

Figure 6. Effect of F_{coll} on the mean agglomerate diameter (a) and on the normalized number of agglomerates (b).

θ was measured from the first frame of the deposited droplet drying experiments described above.

The results of this investigation are presented in form of transient responses of the agglomerate mean diameter in Figure 6a and of the normalized total number of agglomerates (entities) in Figure 6b. For simulations S.M01 to S.M04, the maximal achievable time before computer memory overflow (dual 2.4 GHz processor, 4.0 GB RAM) was ~40 s. Simulations S.M05 to S.M10 could be continued to considerably larger times. However, to facilitate the comparison, the presented results are limited to the first 40 seconds. Figure 6 also shows the limiting case of maximal possible agglomeration rate. At this limit, every droplet produces one successful agglomeration event. The change of the total number of agglomerates N_{agg} with time is then

$$\frac{dN_{agg}}{dt} = -\gamma\, N_{p,0}. \tag{30}$$

This means that every droplet introduced to the system removes one particle from the simulation box, independently of the number of collisions within the bed. Integrating Eq. 30 gives

$$N_{agg} = N_{p,0} - \gamma\, N_{p,0}\, t. \tag{31}$$

The decrease of the number of agglomerates given by Eq. 31 can be also expressed in terms of the increase in agglomerate diameter as

$$\frac{dd_{agg}}{dt} = \frac{\pi}{18}\,\frac{\rho_{p,0}\,(1-\varepsilon_{agg})\,\gamma}{M_{p,0}}\,d_{agg}^4, \tag{32}$$

with the corresponding analytical solution of the form

$$d_{agg} = \left[\frac{1}{{d_{agg,0}}^3} - \frac{\pi}{6}\,\frac{\rho_{p,0}\,(1-\varepsilon_{agg})\,\gamma}{M_{p,0}}\,t\right]^{1/3}, \tag{33}$$

where

$$d_{agg,0} = \left[\frac{{d_{p,0}}^3}{1-\varepsilon_{agg}}\right]^{1/3}. \tag{34}$$

In Figure 6 one can recognize that the simple model represented by Eq. 33 predicts a much higher agglomeration rate than the MC simulations. This is expected because in the MC simulations several factors impede the droplets to form an agglomerate, namely drying of deposited droplets, nonfulfillment of the Stokes criterion and sterical effects, which will be discussed in more detail later on.

Regarding the MC simulations, it is seen that for $F_{coll} > 2820$ the total number of collisions within the bed has no significant influence on the results. On the contrary, for $F_{coll} < 2820$ the agglomeration rate is highly affected by the number of collisions occurring within the fluidized bed. As the number of collisions increases, the time necessary to reach a certain agglomerate diameter is drastically reduced. This means that at very high number of collisions (in this case $F_{coll} > 2820$), as soon as a droplet is deposited on the particle surface, a wet collision takes place. Since the droplet at this stage is fresh, it is very likely that the Stokes criterion will be fulfilled, resulting in an agglomeration event. As the diameter increases and the collision energy becomes larger, the droplets must increase their viscosity before a coalescence can take place. This is the only condition at which the droplets have time to dry at a very high number of collisions.

On the other hand, process kinetics at $F_{coll} < 2820$ is attributed to a coupled effect between the number of wet collisions and the properties of the droplet at collision time. Note that the probability of contact by at least one wet zone is the same for every simulation since it is only influenced by the solid–liquid equilibrium. As the total number of collisions decreases, so does the number of wet collisions and, as a consequence, the number of agglomeration events. This can be easily seen in Figure 7, where the relative number of agglomeration events

$$\eta_{agglo} = \frac{N_{agglo}}{N_{d,tot}} \tag{35}$$

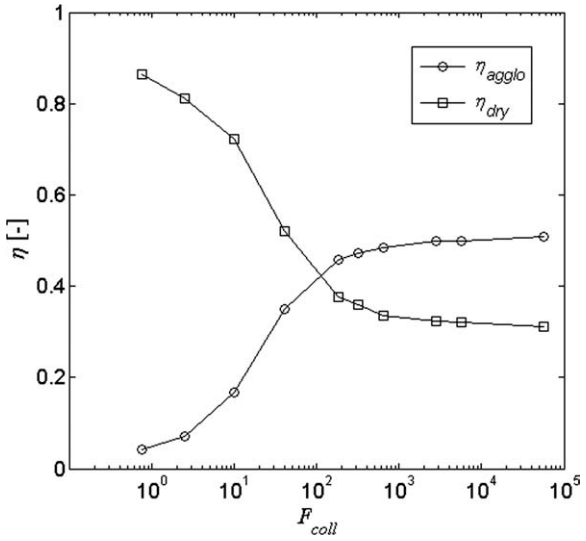

Figure 7. Effect of the length of time step on the fraction of droplets used for agglomeration (η_{agglo}) and on the fraction of evaporated droplets (η_{dry}), Set 1.

is plotted for $t = 40$ s as a function of the collision frequency prefactor. Here N_{agglo} is the total number of agglomeration events and $N_{d,tot}$ is the total number of droplets introduced to the system at certain t described by

$$N_{d,tot} = \gamma\, N_{p,0}\, t. \tag{36}$$

Note that for all cases shown in Table 3 ($N_{p,0} = 2000$ and $\gamma = 0.05\ s^{-1}$), the total number of droplets $N_{d,tot}$ introduced within a period of 40 s equals 4000. The decrease of the number of agglomerations with decreasing number of collisions in Figure 7 is the result of two effects, smaller number of wet collisions and less collisions that satisfy the Stokes criterion.

The relative number of dried droplets (droplets lost by evaporation)

$$\eta_{dry} = \frac{N_{dry}}{N_{d,tot}} \tag{37}$$

at $t = 40\ s$ is additionally presented in Figure 7. It is clearly observed that when the number of collisions decreases, the fraction of droplets being evaporated before a coalescence can occur increases. Note that the droplet drying time is the same for all simulations and equal to $\sim t_{dry} = 3.8$ s when using the drying model according to Eq. 17. It can be also noticed in Figure 7 that the sum of the fractions of used and dried droplets ($\eta_{agglo}+\eta_{dry}$) is less than unity. This is because at any time during the simulation there is a fraction of still liquid droplets in the system. These droplets cannot be accounted in η_{agglo} because they did not yet form a liquid bridge but also cannot be accounted in η_{dry} because they did not yet dry out. Concerning the droplets, they may be at positions that remain accessible after a successful coalescence has occurred, or at positions in the vicinity of the liquid bridge, which are not accessible anymore. This effect is called sterical impediment of deposited droplets. Such sterically impeded droplets will unavoidably dry out because they are not allowed to come in touch with the surface of another particle. When F_{coll} goes to infinity every accessible droplet is consumed by coalescence before it can dry. Consequently, dried droplets at this limit are sterically impeded droplets. Their fraction is given asymptotically to $\eta_{dry} \approx 0.3$ at $F_{coll} \rightarrow \infty$ as Figure 7 shows. Simultaneously, we get $\eta_{agglo} \approx 0.5$. The remaining 20% of the droplets are still liquid, located either at accessible or at sterically impeded positions. The sterical effect explains the deviation of the simple model given by Eq. 33 from the MC simulations even at very high number of interparticle collisions. The fraction of sterically impeded droplets is expected to be less significant as the rate of droplet injection decreases. However, it does not depend on the characteristic drying time, because droplets trapped among the primary particles will anyway dry out.

Then, it can be said that the variation of the number of collisions is always accompanied by a relative change of droplet properties at the exact moment of collision. When the collisions are rare, the deposited droplet is during the next collision drier than it would have been if the collisions were frequent. This compromises the fulfilment of the Stokes criterion and eventually increases the droplet losses within the system. Then, two limiting cases can be recognized. When the collisions are frequent, the deposited droplet drying mechanism can be neglected. In this case, the process is solely governed by the droplet addition rate and the probability of wet collision. The Stokes criterion starts playing a role only when the agglomerates get bigger. On the other hand, when the collisions are rare the total number of wet collisions decreases and the drying mechanism becomes important. Under these conditions, the satisfaction of the Stokes criterion is crucial from the very beginning of the process. For all the cases in between, the influences of these characteristic times are coupled and their relationship complex.

Figures 6 and 7 show that the effect of the number of collisions can be neglected for $F_{coll} > 2820$. However, it can be inferred that this behavior changes as the drying time of the deposited droplets varies, e.g. by manipulating the process temperature or the fluidization gas flow. Additionally, there is a third characteristic quantity playing a role in the process, namely the droplet addition time t_{ad}. This is the time necessary to introduce one single droplet to the simulation, as described by Eq. 6. A change of t_{ad} may significantly affect the relationship between the drying and collision times, and their effect on agglomeration. To analyze the possible effect of the relationship between the collision t_{step}, drying t_{dry} and addition t_{ad} times, two further sets of simulations were performed, denoted by Set 2 and Set 3 in Table 5. For the variation of the drying time, Set 1 is taken as a base case and compared with Set 2 in which t_{dry} is reduced to 1 s keeping constant the droplet addition time t_{ad}. For the manipulation of the addition time, the base case was compared with Set 3. The latter has an addition time 20 times

Table 5. Simulation Parameters for the Investigation of the Coupled Effect of Drying and Addition Times

Set	t_{dry} (s)	γ (s^{-1})	t_{ad} (s)	F_{coll} (m^{-1})	$N_{d,tot}$ at 40 s
1	3.8	0.0500	0.01	56400–0.75	4000
2	1.0	0.0500	0.01	56400–0.75	4000
3	3.8	0.0025	0.20	56400–0.75	200

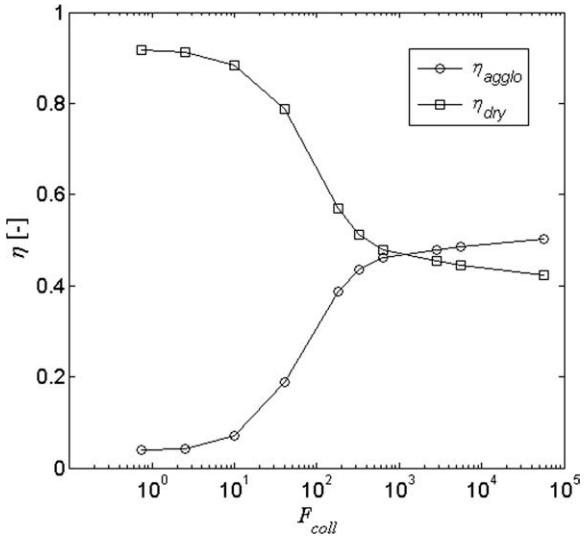

Figure 8. Effect of the length of time step on the fraction of droplets used for agglomeration (η_{agglo}) and on the fraction of evaporated droplets (η_{dry}), Set 2.

larger than Set 1, which means that much less droplets are given to the system. The droplet drying time is equal for Set 1 and Set 3.

Figures 8 and 9 present the number of agglomerations and dried droplets for Set 2 and Set 3 as a function of the number of collisions among the particles (Set 1 has already been given by Figure 7). As it can be observed in Figure 8, Set 2 shows the same qualitative tendencies as Figure 7, Set 1. The more collisions take place within the bed, the higher is the fraction of agglomerations and the smaller is the fraction of dry droplets. However, by comparing Figure 7 and Figure 8 for the same number of collisions, it can be seen that when the droplets dry faster, the fraction of dried droplets increases and the number of agglomerations decreases. While for Set 1 the effect of the number of collisions within the bed can be neglected for $F_{coll} > 2820$, for $t_{dry} = 1$ s it is rather important during the whole range of tested values (no constant values are reached). This confirms that the smaller the drying time of the droplets, the higher is the effect of the number of collisions between the particles on the agglomeration behavior.

The effect of the addition time and the collision time is obtained when comparing Figure 7, Set 1 and Figure 9, Set 3. As these sets of simulations were performed with the same droplet drying time, the difference between the systems is only attributed to the significantly different number of droplets introduced to the system ($N_{d,tot} = 4000$ for Set 1 and $N_{d,tot} = 200$ for Set 3 within a period of 40 s). As it can be observed in Figure 9, the effect of the total number of collisions between the particles can be neglected far before when less droplets are fed to the simulation (limiting value for $F_{coll} > 320$). Figure 9 furthermore shows that the minimum fraction of lost droplets η_{dry} is close to 0.05 for the given conditions (compare with $\eta_{dry} \approx 0.3$ for Set 1). As already discussed, this asymptotic value represents the number of droplets that dry while trapped inside the agglomerate structure due to the spatial arrangement of the particles forming the agglomerate. This fact supports the hypothesis that the rate of droplet addition influences the maximum percentage of droplets that can be used for agglomeration. Recall, however, that these are relative quantities, so that the total number of agglomerations is still much higher in Set 1 and Set 2 than in Set 3. On the one hand, the fraction of droplets lost by drying increases when increasing the droplet addition rate. On the other hand, systems with more deposited droplets show higher agglomeration rates.

The discussed results indicate that the effect of the number of collisions, represented by the collision frequency, is more important for smaller drying times and higher number of sprayed droplets. It can be concluded that the relationship between the characteristic collision, drying and addition times is complex. The proposed model shows regions of high but also regions of low sensitivity upon these parameters. The reliable determination of the time elapsed between collisions appears to be most important.

However, the determination of characteristic times is demanding, theoretically as well experimentally. A possible way to avoid respective uncertainties is to present the model results as a transient response of the system based on iterations instead of real time. This has been previously done by Thielmann et al.[28] However, with such an approach the comparison of simulation results with experimental agglomeration kinetics and the introduction of the drying mechanism (which is time dependent) are not feasible. To be able to compare the simulation with experimental results in absence of a reliable and experimentally validated collision model, Eq. 27 was applied in this work by adjusting the base simulation to the corresponding experimental results (E.02). Then, an estimate of the number of collisions per particle per second which is assumed as characteristic of the particulate system was accomplished. The best adjustment was

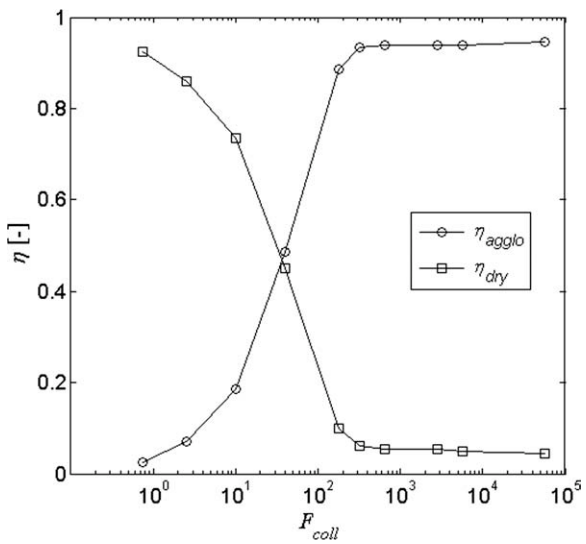

Figure 9. Effect of the length of time step on the fraction of droplets used for agglomeration (η_{agglo}) and on the fraction of evaporated droplets (η_{dry}), Set 3.

Table 6. Simulation Parameters

Parameter			Label
	$\dot{M}_l$ (g/h)	γ (s^{-1})	
Binder addition rate $\dot{M}_l$	100	0.017	S.01
	300	0.050	S.02
	500	0.083	S.03
	x_b (−)	μ_l (Pa s)	
Binder viscosity μ_l	4	0.025	S.04
	8	0.147	S.02
	10	0.322	S.05
	u_0 (m/s)	u_c (m/s)	
Fluidization velocity u_0	0.94	0.47	S.06
	1.35	0.68	S.02
	1.47	0.74	S.07
	$T_{g,in}$ (°C)	T^* (°C)	
Gas inlet temperature $T_{g,in}$	30	14.0	S.05
	50	21.5	S.08
	80	28.5	S.09

obtained for $F_{coll} = 10$ (S.M08). Once fitted, this prefactor was kept constant in all subsequent simulations of this work.

Effect of process parameters

The performance of the model was evaluated by analyzing the effect of variation of process parameters on agglomeration kinetics and comparing the results with selected experiments. These parameters are the binder addition rate, the binder initial viscosity, the superficial fluidization velocity and the gas inlet temperature. The simulation parameters follow the experimental ones presented in Table 2. An overview based on the varied parameters is shown in Table 6.

Effect of Binder Addition Rate. The effect of the binder addition rate (represented in the model by the droplet addition rate) was analyzed by keeping the number of particles constant and varying the number of droplets introduced into the system according to the binder mass flow rate (Eq. 5). The simulations for this investigation correspond to S.01, S.02 and S.03. Figure 10 shows the response of the median agglomerate diameter as the binder addition rate is varied and the comparison with the corresponding experiments. As it can be observed, the agglomeration rate is proportional to the number of droplets introduced to the system. The more wet spots are produced on the particle surface, the higher is the probability of wet collision. This leads to the formation of more liquid bridges between the particles and allow them to grow to larger sizes within a shorter period of time.

An additional important feature of the model proposed in this study is the possibility of obtaining distributed properties of the agglomerates, such as the particle size distribution (PSD), which is otherwise achievable only by complicated solutions of multivariant PBE. As an example, the modeled and experimentally obtained cumulative particle size distributions ($t = 90$ s) for the above mentioned simulations and experiments are given in Figure 11a,b, respectively. There it can be seen that the model predicts a broader particle size distribution as the amount of injected binder increases, which was also experimentally observed.

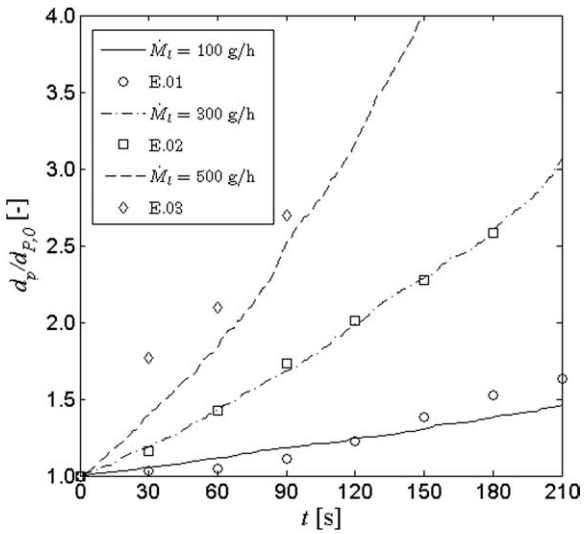

Figure 10. Effect of the binder addition rate on the agglomerate growth rate.

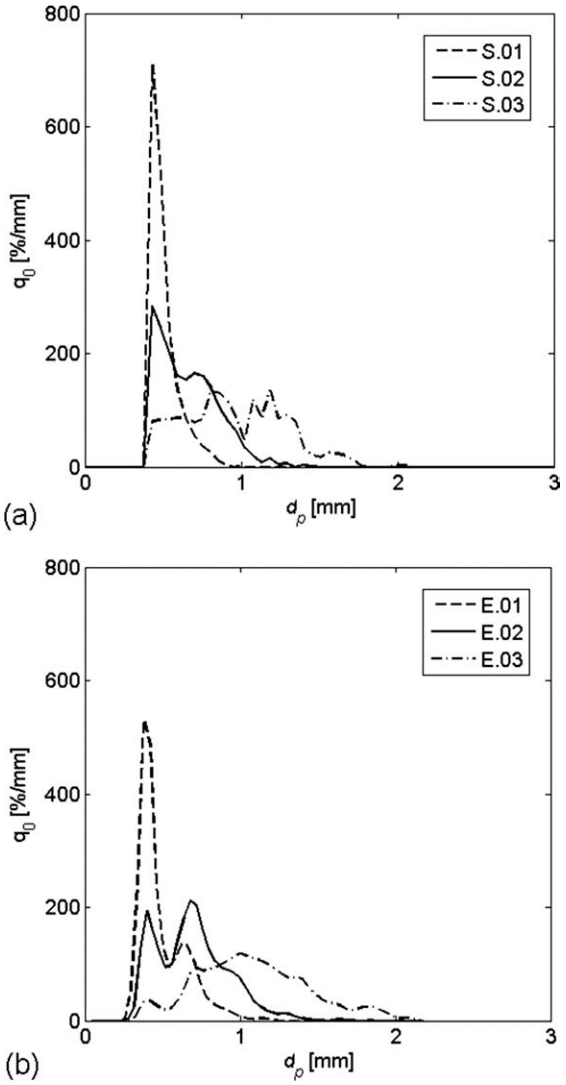

Figure 11. Effect of the binder addition rate on the PSD, comparison of simulations (a) with experiments (b) at $t = 90$ s.

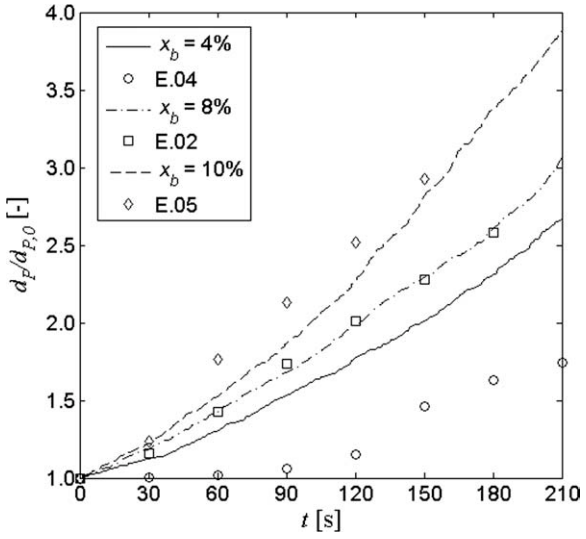

Figure 12. Effect of the binder viscosity on the agglomerate growth rate.

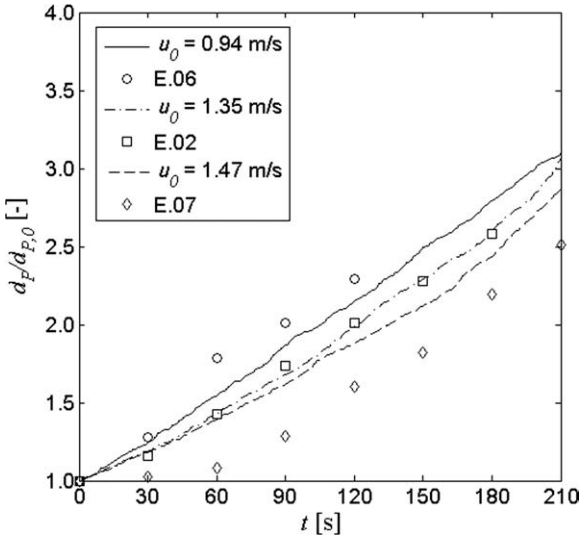

Figure 13. Effect of the superficial fluidization velocity on the agglomerate growth rate.

Effect of Binder Viscosity. To study the effect of the initial binder viscosity on the process, simulations with different inlet binder mass fractions, $x_b = 4$, 8, and 10%, were performed corresponding with experiments E.04, E.02, and E.05, respectively. The results are presented in Figure 12. Increasing the binder viscosity causes an increase of the agglomeration speed. This can be explained by the fact that a more viscous liquid layer is able to dissipate a higher fraction of the collision energy. This guarantees that a higher number of collisions fulfills the Stokes criterion and, therefore, more agglomeration events are observed. Additionally, as the particles grow and become heavier, the energy of collision increases; low viscosity binders are not able to absorb this energy, producing a higher number of rebounds.

Effect of Fluidization Velocity. According to the Stokes criterion presented (Eqs. 10–13), the fraction of the collision energy that a liquid layer is able to dissipate to produce coalescence is directly related to the collision velocity of the pair of particles. Since u_c is correlated with the superficial gas velocity u_0, simulations at different fluidization velocities were performed and compared with experiments in Figure 13.

As it can be seen, the model anticipates the experimentally observed decrease of the maximum attainable agglomerate diameter as gas velocity increases. The explanation to this phenomenon involves several factors. Firstly, in the presented model and according to Eq. 27, an increase of the fluidization velocity means a higher number of interparticle collisions (smaller characteristic collision time t_{step}). This leads to higher number of agglomerations per unit time and increases the agglomeration rate under otherwise identical conditions (Figure 7). On the other hand, more air flow decreases the characteristic drying time t_{dry} of the deposited droplet, eventually reduces the availability of wet zones in the system and depletes the number of agglomerations. This was already demonstrated by comparing Figures 7 and 8. A third important factor is that the fluidization velocity is directly proportional to the collision velocity. According to the Stokes criterion, as the collision energy increases, the ability of the liquid layer to completely dissipate the kinetic energy is reduced. Thus, less wet collisions lead to successful agglomeration. In total, the experimental tendency of smaller agglomeration rate at higher gas velocity is the result of these three competing phenomena; more collisions are observed (smaller t_{step}), a smaller fraction of them takes place on a wet region (smaller t_{dry}) and the Stokes criterion is more difficult to fulfill. It is obvious that, for the tested system, the positive effect of more collisions was overcome by faster drying and higher collision energies.

Thermal effects

Effect of Drying Mechanism. The proposed model allows to analyze the role of mechanisms that directly affect the agglomeration behavior but are very difficult, if not impossible, to isolate in the real process. Such a mechanism is drying. The influence of deposited droplet drying mechanism on the agglomeration behavior is analyzed by taking two limiting cases. The first case corresponds to the assumption that, once the droplet is deposited, no drying is observed (simulations labeled as ND). The second case corresponds to the drying model, Eq. 17, which considers the fluidized bed as a well mixed medium where the bulk gas moisture content is equal to the outlet moisture content. The simulations are performed with an initial gas temperature equal to $T_g = 30°C$ and $u_0 = 1.35$ m/s, which results in a characteristic drying time of $t_{dry} = 3.8$ s. Binder of different initial viscosities is used as it is given in Table 7.

The results are presented in Figure 14 where two tendencies can be identified. For low-viscosity binders ($x_b = 2\%$),

Table 7. Initial Values of Stokes Number as Function of Binder Viscosity

x_b (−)	μ_l (Pa s)	$St_{coal,0}$	$St^0_{coal,0}$
2	0.009	8.37	2.31
8	0.147	0.49	2.31
10	0.322	0.22	2.31

the inclusion of the drying mechanism represents a considerable improvement to the agglomeration rate. When drying is not included, no size enlargement is observed. On the contrary, with viscous binders ($x_b \geq 8\%$) smaller agglomeration rates are obtained when drying is implemented. These opposite trends can be explained by taking a look at the values of the initial Stokes and critical Stokes numbers for each case given in Table 7 ($h_0 = 0.0279$ mm, $d_d = 80$ μm and $\theta = 40°$). For low viscosity binders ($x_b = 2\%$), the initial value of the Stokes number lies over the coalescence limit, which means that under these circumstances no agglomeration can take place. However, as the droplets are allowed to dry, their viscosity increase, and at certain point the layer is viscous enough to dissipate the collision energy and produce coalescence. Although a considerable number of droplets are lost by drying in comparison with the nondrying case, the positive effect of the increase in viscosity is much stronger. On the other side, when the initial Stokes number is smaller than the critical value (high binder viscosities), the deposited layer is already able to dissipate the energy, so that the effect of increasing binder viscosity during drying does not play an important role. In these cases, the implementation of drying means a reduction of the droplet availability in the system and the agglomeration rate is reduced.

This demonstrates the importance of drying in wet agglomeration and leads to the conclusion that both mechanisms, agglomeration and drying, are coupled to each other. It also shows that drying of deposited droplets does not necessarily mean a reduction of the agglomeration rate. Since drying is governed mainly by the gas inlet temperature, its effect is further discussed in the next section.

Effect of Gas Inlet Temperature. To investigate the influence of gas inlet temperature on the agglomeration behavior, a set of simulations and experiments varying this parameter and keeping constant all other variables was carried out. The experiments correspond to E.05, E.08, and E.09 at $T_{g,in} = 30$, 50, and 80°C, respectively. Figure 15 presents the simulation results and the comparison with the experiments. It is seen that, high gas inlet temperatures result in lower agglomeration rates in the experiments as well as in the simulations. This can be explained by the significantly different characteristic drying times of the deposited droplets $t_{dry} = 3.8$ s, 1.8 s and 1.1 s for $T_{g,in} = 30$, 50 and 80°C, respectively. As the gas inlet temperature is increased, the time that a droplet is able to expend deposited on the particle before total evaporation is considerably reduced. This means that less droplets are available in the system to form a bridge. Due to the considerably smaller number of wet collisions, the number of coalescence events is depleted. These results explain the empirically known influence of process temperature on the agglomeration of nonsintering products based solely on microscale interactions.

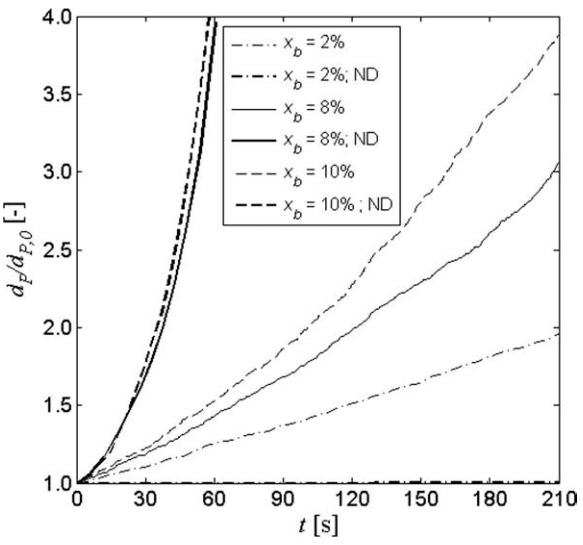

Figure 14. Effect of the deposited droplet drying mechanism on the agglomeration behavior.

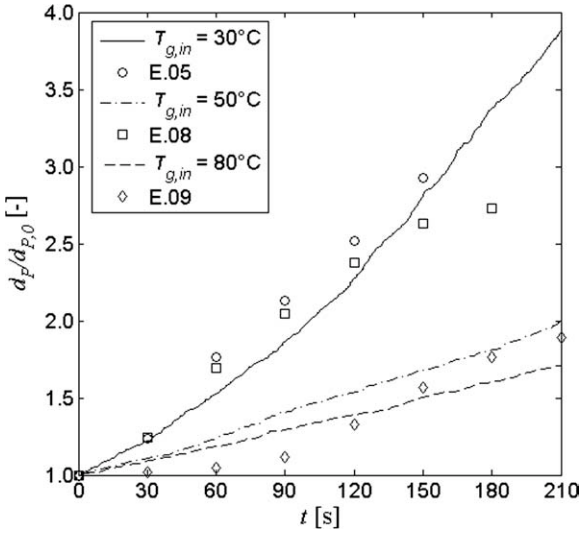

Figure 15. Effect of gas inlet temperature on the agglomerate diameter.

Conclusions

A microscale model that provides a better understanding of the agglomeration kinetics in fluidized beds has been presented. The model accounts for discrete interactions among the main entities within the fluidized bed, namely primary particles and droplets, which generate events that result in a particle enlargement process. These events are interparticle collisions, sprayed droplet capture, particle wetting, deposited droplet aging by drying as well as coalescence or rebound after collision. The solid particles are assumed to be spherical and nondeformable.

The sensitivity of the model to changes of the most important characteristic times, namely the droplet addition time, the drying time and the collision time was evaluated. The results show that the number of collisions within the bed, directly related to the collision time, plays a very important role in the process, as it may govern the number of possible agglomeration events per unit time and the extent of the influence of the drying mechanism.

As the number of collisions that a single particle undergoes per unit time increases, the droplets deposited on its surface do not have enough time to dry before a bridge is produced. This reduces significantly the number of droplets

lost by drying and eventually increases the number of coalescence events, resulting in larger agglomeration rates. On the other hand, when the number of collisions is reduced, the droplets experience aging before a collision occurs; considerably more droplets are then dried before they can contact another agglomerate to produce a coalescence. The number of wet collisions within the bed is influenced by the droplet drying time and, additionally by the droplet addition time. The relative order of magnitude of the mentioned three characteristic times is very important for a reliable simulation of agglomerate formation by the stochastic microlevel approach. In lack of reliable data on collision frequency, the prefactor of an empirical equation from literature was fitted to one selected agglomeration experiment. Collision frequencies resulting from its fitting are relatively moderate, about 2 s^{-1} at the beginning of the process at the investigated conditions.

After the described adjustment, the performance of the model was evaluated by comparison of with lab-scale agglomeration trials under variation of the most important process parameters. The simulations agree with the experimental results, showing that when the amount of binder introduced to the system increases the agglomeration rate is enhanced. A similar tendency is observed when the initial binder viscosity is increased and the superficial fluidization velocity is reduced. While the first influence is related to the number of wet collisions per unit time that the system undergoes, the last two influences are related to the fraction of wet collisions that may lead to a successful agglomeration event. The proposed model enables to obtain distributed properties, such as the particle size distribution.

A clear conclusion of the investigation is that drying and size enlargement are closely connected to each other in wet agglomeration processes. The influence of the drying mechanism can be quantified and the effect of process temperature on agglomeration kinetics can be explained based exclusively on microscale physical mechanisms. At high drying rates, namely at high process temperatures, the drying time of the droplets is reduced. This depletes the number of wet collisions and usually slows down the agglomeration speed. However, drying can also have the opposite influence, triggering agglomeration by increasing viscosity of initially thin binder solutions.

The proposed methodology appears to be a worthy alternative to traditional approaches used for the treatment of agglomeration processes because it gives the correct response to changes of process variables and, on the other hand, enables the study of intrinsic, otherwise hardly accessible mechanisms.

Acknowledgments

K.T.-V. was supported by CONACyT (Mexico) and DAAD (Germany). Experimental facilities have been founded by DFG (Germany), PE1423/1-1.

Notation

a = base radius of spherical cap (m)
A = area (m^2)
Ar = Archimedes number (-)
d = diameter (m)
e = restitution coefficient (-)
f_{coll} = collision frequency (1/s)
F_{coll} = collision frequency prefactor (1/m)
g = gravity (m^2/s)
h = binder layer thickness (m)
h_a = height of particle surface asperities (m)
i = colliding pair (-)
I = non-Newtonian index (-)
k = event (-)
l = characteristic length (m)
M = mass (kg)
$\dot{M}$ = mass flow rate (kg/s)
$\tilde{M}$ = molecular weight (kg/kmol)
N = number (-)
$\dot{N}_d$ = droplet flow rate (1/s)
N_p = number of particles in simulation box (-)
$\mathcal{N}$ = number of doublings (-)
p = number of positions on the particle surface (-)
P = pressure (Pa)
P_v^* = saturation vapor pressure (Pa)
q_0 = number density size distribution (1/m)
Q_0 = number density cumulative particle size distribution (%)
Re = Reynolds number (-)
St_{coal} = Stokes coalescence number (-)
St_{coal}^* = Stokes coalescence critical number (-)
t = time (s)
T = temperature (°C)
u_c = collision velocity (m/s)
u_0 = fluidization gas velocity (m/s)
V = volume (m^3)
x_b = binder mass fraction (-)
$\tilde{y_g}$ = molar fraction in the gas phase (-)
Y = moisture content, dry basis (g/kg)

Greek letters

β = mass transfer coefficient (m/s)
γ = droplet addition rate (1/s)
ε = voidage (-)
η = relative number of events (-)
θ = contact angle (°)
μ = viscosity (Pa s)
ρ = density (kg/m^3)
σ_{uc} = collision velocity standard deviation (m/s)
ϕ = solid volume fraction (-)
Φ_s = fractional covered area by a single droplet (-)

Subscripts

agg = agglomerate
agglo = agglomeration event
ad = addition
b = solute
cap = spherical cap, deposited droplet
coll = collision
d = droplet
dry = drying
exp = expanded bed
fix = fixed bed
g = gas
in = inlet
p = particle
tot = total
w = water
0 = initial
* = saturation

Abbreviations

FB = fluidized bed
HPMC = hydroxypropyl-methylcellulose
MC = Monte Carlo
SD = single droplet
ND = no drying
PBE = population balance equations
PSD = particle size distribution

Literature Cited

1. Pietsch W. *Size Enlargement by Agglomeration*. New York: Wiley, 1991.
2. Litster J, Ennis B. *The Science and Engineering of Granulation Processes*. Dordrecht: Kluwer, 2004.
3. Pietsch W. *Agglomeration in Industry. Occurrence and Applications*. Weinheim: Wiley-VCH, 2005.
4. Gibson M. *Pharmaceutical Preformulation and Formulation. A Practical Guide From Candidate Drug Selection to Commercial Dosage Form*. Boca Raton: Interpharm CRC, 2004.
5. Ramkrishna D. *Population Balances: Theory and Applications to Particulate Systems in Engineering*. New York: Academic Press, 2000.
6. Heinrich S, Peglow M, Ihlow M, Henneberg M, Mörl L. Analysis of the start-up process in continuous fluidized bed spray granulation by population balance modelling. *Chem Eng Sci*. 2001;57:4369–4390.
7. Peglow M, Kumar J, Warnecke G, Heinrich G, Tsotsas E, Morl L, Hounslow MJ. An improved discretized tracer mass distribution of Hounslow et al. *AIChE J*. 2006;52:1326–1332.
8. Terrazas-Velarde K, Peglow M, Tsotsas E. Stochastic simulation of agglomerate formation in fluidized bed spray drying: a micro-level approach. *Chem Eng Sci*. 2009;64:2631–2643.
9. Metropolis N, Ulam S. The Monte Carlo method. *J Am Stat Asocc*. 1949;44:335–341.
10. Ramkrishna D. Analysis of population balance-IV. The precise connection between Monte Carlo simulation and population balances. *Chem Eng Sci*. 1981;36:1203–1209.
11. Zhao H, Maisels A, Matsoukas T, Zheng CG. Analysis of four Monte Carlo methods for the solution of population balances in dispersed systems. *Powder Technol*. 2007;173:38–50.
12. Tan HS, Salman AD, Hounslow MJ. Kinetics of fluidised bed melt granulation I: the effect of process variables. *Chem Eng Sci*. 2006;61:1585–1601.
13. Yang W. *Handbook of Fluidization and Fluid Particle Systems*. New York: Marcel Dekker Inc., 2003.
14. Heinrich S, Blumschein J, Henneberg M, Ihlow M, Peglow M, Mörl L. Study of dynamic multi-dimensional temperature and concentration distributions in liquid-sprayed fluidized beds. *Chem Eng Sci*. 2003;58:5135–5160.
15. Clarke A, Blake TD, Carruthers K, Woodward A. Spreading and imbibition of liquid droplets on porous surfaces. *Langmuir*. 2002; 18:2980–2984.
16. Ennis BJ, Tardos G, Pfeffer R. A microlevel-based characterization of granulation phenomena. *Powder Technol*. 1991;65:257–272.
17. George DC, Johri J, Goldfarb D. Dependence of particle fluctuation velocity on gas flow, and particle diameter in gas fluidized beds for monodispersed spheres in the Geldart B and A fluidization regimes. *Powder Technol*. 2008;182:146–170.
18. Erbil HY, McHale G, Newton MI. Drop evaporation on solid surfaces: constant contact angle mode. *Langmuir*. 2002;18:2636–2641.
19. Schlünder EU, Tsotsas E. *Wärmeübertragung in Festbetten, durchmischten Schüttgütern und Wirbelschichten*. Stuttgart: Thieme Verlag, 1998.
20. Buffière P, Moletta R. Collision frequency and collisional particle pressure in three-phase fluidized beds. *Chem Eng Sci*. 2000;55: 5555–5563.
21. Hampel R, Peglow M, Kumar J, Tsotsas E, Heinrich S. Study of agglomeration kinetics in fluidized beds referring to the moisture content of particles. In: *Proceedings of the third International Conference on Population Balance Modeling*, Quebec/Canada; September 18–21, 2007.
22. Aulton M, Twichell AM, Hogan JE. Physical properties of HPMC solutions and their role in the film coating process and the quality of the coated product. In: McGinity JW, editor. *Aqueous Polymeric Coating for Pharmaceutical Dosage Forms*, 2nd ed. New York: Marcel Dekker, 1997:227–266.
23. Nagai T, Obara S, Kokubo H, Hoshi N. Application of HPMC and HPMCAS to aqueous film coating of pharmaceutical dosage forms. In: McGinity JW, editor. *Aqueous Polymeric Coating for Pharmaceutical Dosage Forms*, 2nd ed. New York: Marcel Dekker, 1997: 177–225.
24. Utikar RP, Ranade VV. Single jet fluidized beds: experiments and CFD simulations with glass and polypropylene particles. *Chem Eng Sci*. 2007;62:167–183.
25. Sommerfeld M, Huber N. Experimental analysis and modelling of particle-wall collisions. *Int J Multiphase Flow*. 1999;25:1457–1489.
26. Weber S, Briens C, Berruti F, Chan E, Gray M. Agglomerate stability in fluidized beds of glass beads and silica sand. *Powder Technol*. 2006;165:115–127.
27. Jiménez T, Turchiuli C, Dumoulin E. Particles agglomeration in a conical fluidized bed in relation with air temperature profiles. *Chem Eng Sci*. 2006;61:5954–5961.
28. Thielmann F, Naderi M, Ansari M, Stepanek F. The effect of primary particle surface energy on agglomeration rate in fluidized bed wet granulation. *Powder Technol*. 2008;181:160–168.

Manuscript received Jun. 8, 2010, revision received Oct. 22, 2010, and final revision received Dec. 6, 2010.